Обзор ArXiv: astro-ph, 18-22 декабря 2017 года

От Сильченко О.К.

Astro-ph: 1712.05833

The extended Planetary Nebula Spectrograph (ePN.S) early-type galaxy survey. The kinematic diversity of stellar halos and the relation between halo transition scale and stellar mass

C. Pulsoni[1,2], O. Gerhard[1], M. Arnaboldi[3], L. Coccato[3], A. Longobardi[5], N. R. Napolitano[6], C. Narayan[1,8], V. Gupta[1,7], A. Burkert[4], M. Capaccioli[9], A. L. Chies-Santos[10], A. Cortesi[11], K. C. Freeman[12], K. Kuijken[13], M. R. Merrifield[14], A. J. Romanowsky[15,16], and C. Tortora[17]

[1] Max-Planck-Institut für extraterrestrische Physik, Giessenbachstraße, 85748 Garching, Germany
[2] Excellence Cluster Universe, Boltzmannstraße 2, 85748, Garching, Germany
[3] European Southern Observatory, Karl-Schwarzschild-Straße 2, 85748 Garching, Germany
[4] University Observatory Munich, Scheinerstraße 1, 81679 Munich, Germany
[5] Kavli Institute for Astronomy and Astrophysics, Peking University, 5 Yiheyuan Road, Haidian District, Beijing 100871, PR China
[6] INAF - Astronomical Observatory of Capodimonte, Salita Moiariello, 16, 80131, Naples, Italy
[7] Department of Physics, Cornell University, Ithaca, New York 14853, USA
[8] Current address: 71, Akashganga IUCAA Post Bag 4, Ganeshkhind Pune University Campus, Pune - 411007, India
[9] University of Naples "Federico II", C.U. Monte Sant'Angelo, via Cinthia, I-80126, Naples, Italy
[10] Departamento de Astronomia, Instituto de Fsica, Universidade Federal do Rio Grande do Sul, Porto Alegre, R.S 90040-060, Brazil
[11] Departamento de Astronomia, Instituto de Astronomia, Geofisica e Ciencias Atmosfericas da USP, Cidade Universitaria, CEP:05508900 Sao Paulo, SP, Brazil
[12] Research School of Astronomy and Astrophysics, Mount Stromlo Observatory, Cotter Road, Weston Creek, ACT 2611, Australia
[13] Leiden Observatory, Leiden University, PO Box 9513, NL-2300 RA Leiden, the Netherlands
[14] School of Physics and Astronomy, The University of Nottingham, University Park, Nottingham, NG7 2RD, UK
[15] Department of Physics and Astronomy, San Jose State University, One Washington Square, San Jose, CA 95192, USA
[16] University of California Observatories, 1156 High Street, Santa Cruz, CA 95064, USA
[17] Kapteyn Astronomical Institute, University of Groningen, Postbus 800, NL-9700 AV Groningen, the Netherlands

December 19, 2017

33 галактики ранних типов

Table 1. Properties of the ETG sample analyzed in this paper, and list of references

Galaxy NGC	M_K[a] [mag]	D[b] [Mpc]	class[c]	R_e[d] [arcsec]	R_{max}/R_e[e]	PA_{phot}[f] [degrees]	ϵ[g]	N_{PNe}[h]	References[i] PN data	References[l] abs.line data
0584	−24.23	20.2	F	33 (1)	7.4	63	0.339	25	(7)	(21)
0821	−23.99	23.4	F	40 (2)	4.8	31.2	0.35	122	(8)	(18);(40);(41)
1023	−23.89	10.5	F	48 (2)	6.8	83.3	0.63	181	(8);(9)	(18);(30)
1316	−26.02	21.0	F	109 (3)	4.7	50	0.29*	737	(10)	(22)
1344	−24.21	20.9	F	30 (4)	7.8	167	0.333	192	(12)	(23)
1399	−25.29	20.9	S	127 (3)	4.	110	0.1*	145	(11)	(24)
2768	−24.77	22.4	F	63 (2)	6.2	91.6	0.57	312	(9)	(18);(31)
2974	−23.76	22.3	F	38 (2)	5.8	44.2	0.37	22	(7)	(18)
3115	−24.02	9.5	F	93 (6)	4.7	43.5	0.607	183	(9)	(18);(25)
3377	−22.78	11.0	F	35.5 (2)	7.7	46.3	0.33	136	(8)	(18); (33)
3379	−23.80	10.3	F	40 (2)	5.3	68.2	0.13*	189	(8)	(19);(32);(40)
3384	−23.51	11.3	F	32.5 (2)	6.8	53	0.5	85	(9)	(19)
3489	−23.04	12.0	F	22.5 (2)	4.8	70.5	0.45	57	(9)	(19)
3608	−23.69	22.8	S	29.5 (2)	8.2	82	0.2*	92	(8)	(18)
3923	−25.33	23.1	S	86.4 (1)	4.9	48	0.271	99	(15)	(26)
4278	−23.80	15.6	F	31.5 (2)	7.6	39.5	0.09*	69	(7)	(18)
4339	−22.62	17.0	F	30 (2)	3.	15.7	0.07*	44	(7)	(20);(38)
4365	−25.19	23.1	S	52.5 (2)	5.6	40.9	0.24*	227	(7)	(18)
4374	−25.12	18.5	S	52.5 (2)	5.9	128.8	0.05*	445	(8)	(18)
4472	−25.73	16.7	S	95.5 (2)	8.4	154.7	0.19*	431	(7)	(20);(37)
4473	−23.76	15.2	F	27. (2)	5.6	92.2	0.43	153	(7)	(18)
4494	−24.17	17.1	F	49 (2)	4.8	176.3	0.14*	255	(8)	(18);(36)
4552	−24.32	16.0	S	34. (2)	9.2	132	0.11*	227	(7)	(19);(38)
4564	−23.10	15.9	F	20.5 (2)	6.5	48.5	0.53	47	(8)	(18)
4594	−24.93	9.5	F	102 (5)	4.	88	0.521	258	(16)	(27)
4636	−24.35	14.3	S	89. (2)	3.	144.2	0.23*	189	(7)	(20);(39)
4649	−25.35	16.5	F	66 (2)	4.5	91.3	0.16*	281	(13)	(18);(34)
4697	−24.14	12.5	F	61.5 (1)	4.5	67.2	0.32	525	(14)	(18);(35)
4742	−22.60	15.8	F	14.4 (4)	13.1	80	0.351	64	(7)	(28)
5128	−24.16	4.1	F	162.6 (1)	11.9	30	0.069*	1222	(17)	(29)
5846	−25.04	24.6	S	59 (2)	4.3	53.3	0.08*	118	(8)	(18)
5866	−23.99	14.8	F	36 (2)	9.4	125	0.58	150	(7)	(18)
7457	−22.38	12.9	F	36 (2)	3.2	124.8	0.47	108	(9)	(18)

Маятник качнулся в сторону триаксиальных сфероидов?

6.4.4. Summary

We can conclude that a total of 17 galaxies (50%) of the ePN.S sample show smoothed velocity fields that reveal their triaxial nature. 7 objects (4 fast and 3 slow rotators) have significant kinematic twists, and 8 (4 fast and 4 slow rotators) show a significant constant misalignment of $PA_{\rm kin}$ with $PA_{\rm phot}$. In addition two slow rotators have a kinematically decoupled halo.

The observed features are more than 2 sigma significant for most of the cases (1.3 sigma for NGC 4742 and 1.7 sigma for NGC 5846), and they are not effects of the folding operation on the catalogs nor of the smoothing procedure.

All in all, we found that all the slow rotators and 8 out of 24 fast rotators show indications of intrinsic triaxial morphology in the PN data.

Кривые вращения

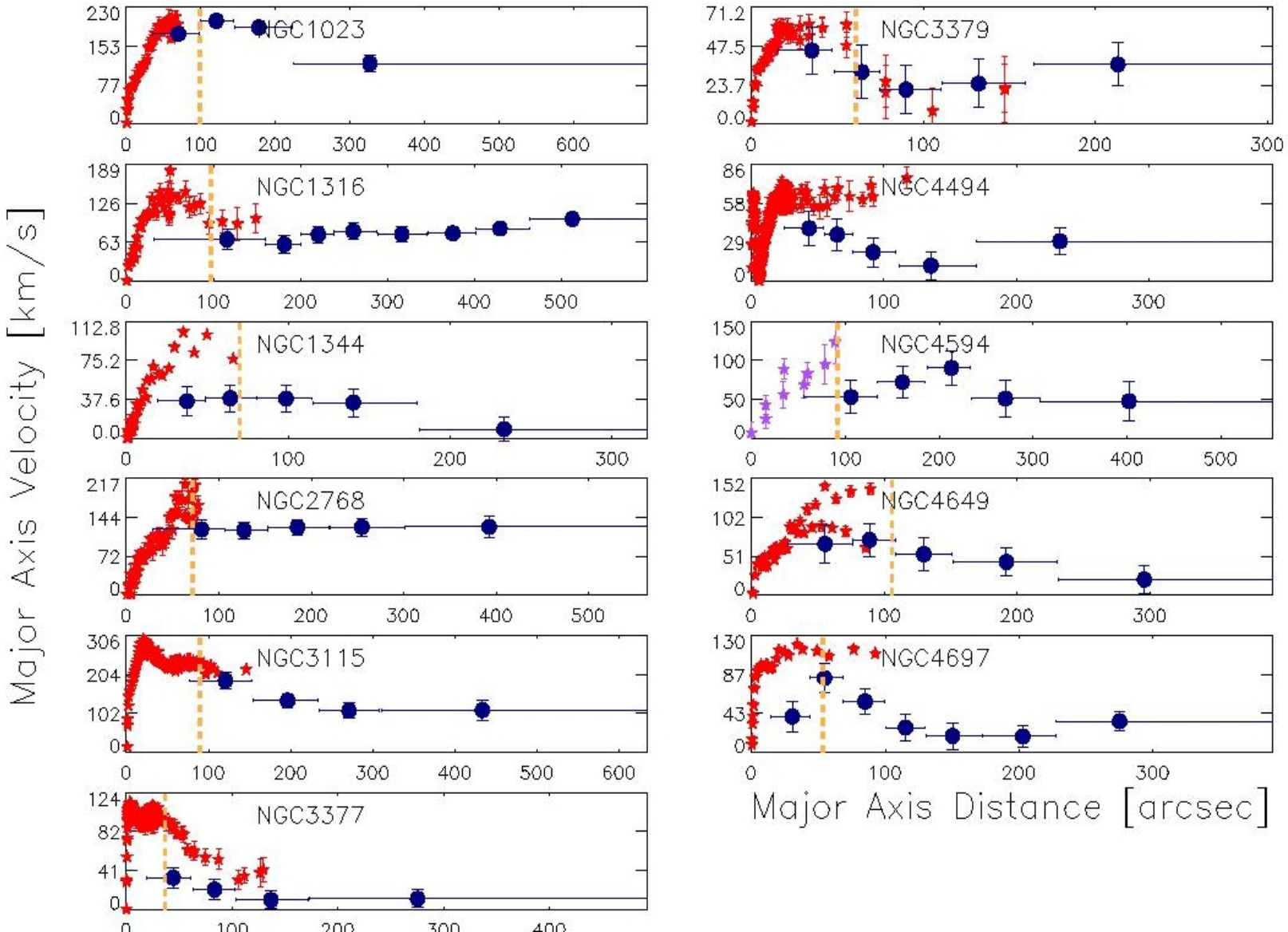

Статистика по скоростям вращения внутренних и внешних областей

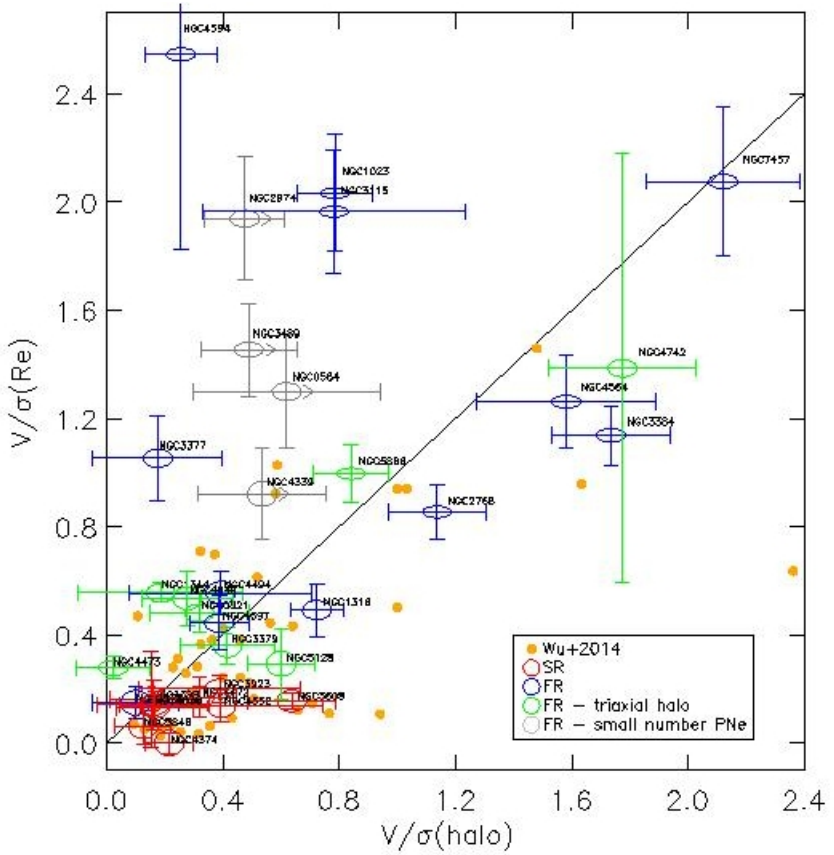

Fig. 7. $V/\sigma(R_e)$ from absorption line data compared with V/σ(halo) from PN data. References for the absorption line data are in table 1; note that for NGC 1399 and NGC 3923 data are available up to $R_e/2$ and $R_e/4$, respectively. The flattening of the ellipses used to plot the galaxies correspond to the ϵ values of table 1. Fast and slow rotators are shown with different colors, as are the triaxial fast rotators. The gray

Словесная формулировка того же самого

In the data presented here, we see

- slow rotators
- fast rotators without apparent disks (NGC 4494 and NGC 4742)
- fast rotators with only inner disks and slowly rotating spheroids (e.g. NGC 3377)
- fast rotators with dominant disks all the way to their outermost regions (e.g. NGC 7457)
- fast rotators with inner disks and rapidly rotating spheroids (e.g. NGC 2768)
- fast rotators with triaxial halos that are dominated by dispersion (e.g. NGC 4649) or that rotate rapidly (NGC 4742 and NGC 5866)

Пример S0

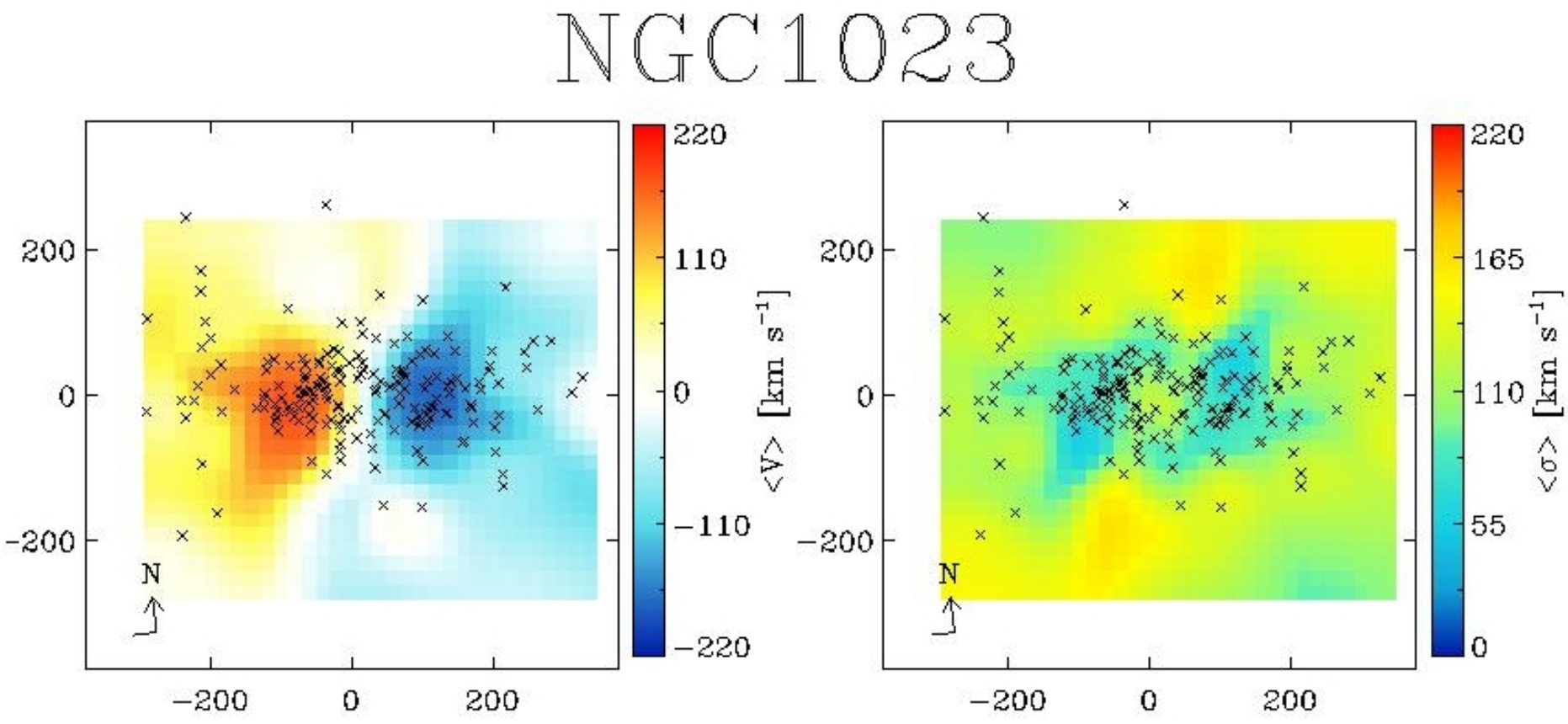
NGC1023
200
0
−200
N
−200
0
200
220
110
0
−110
−220
<V> [km s^{-1}]
200
0
−200
N
−200
0
200
220
165
110
55
0
<σ> [km s^{-1}]

Пример S0 с полярным диском

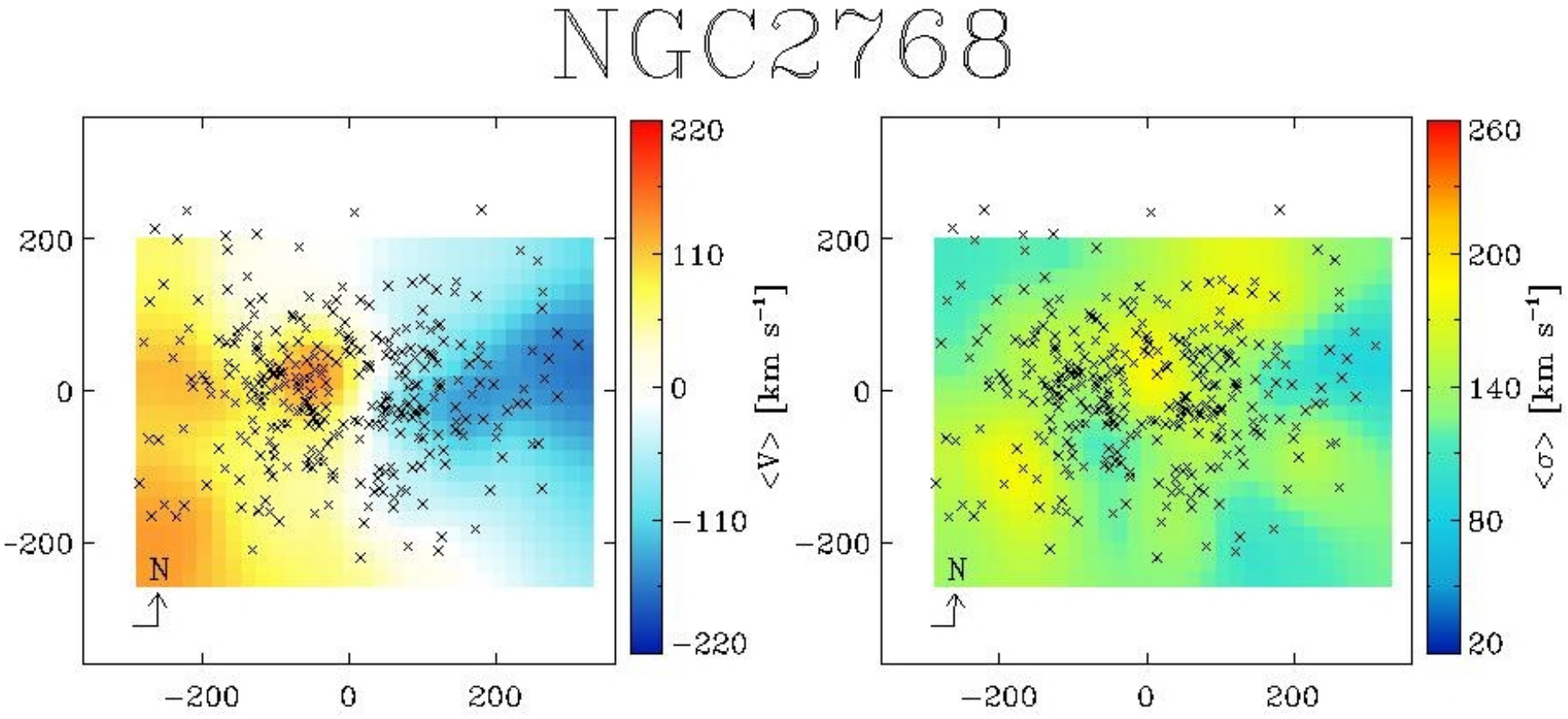

Пример E

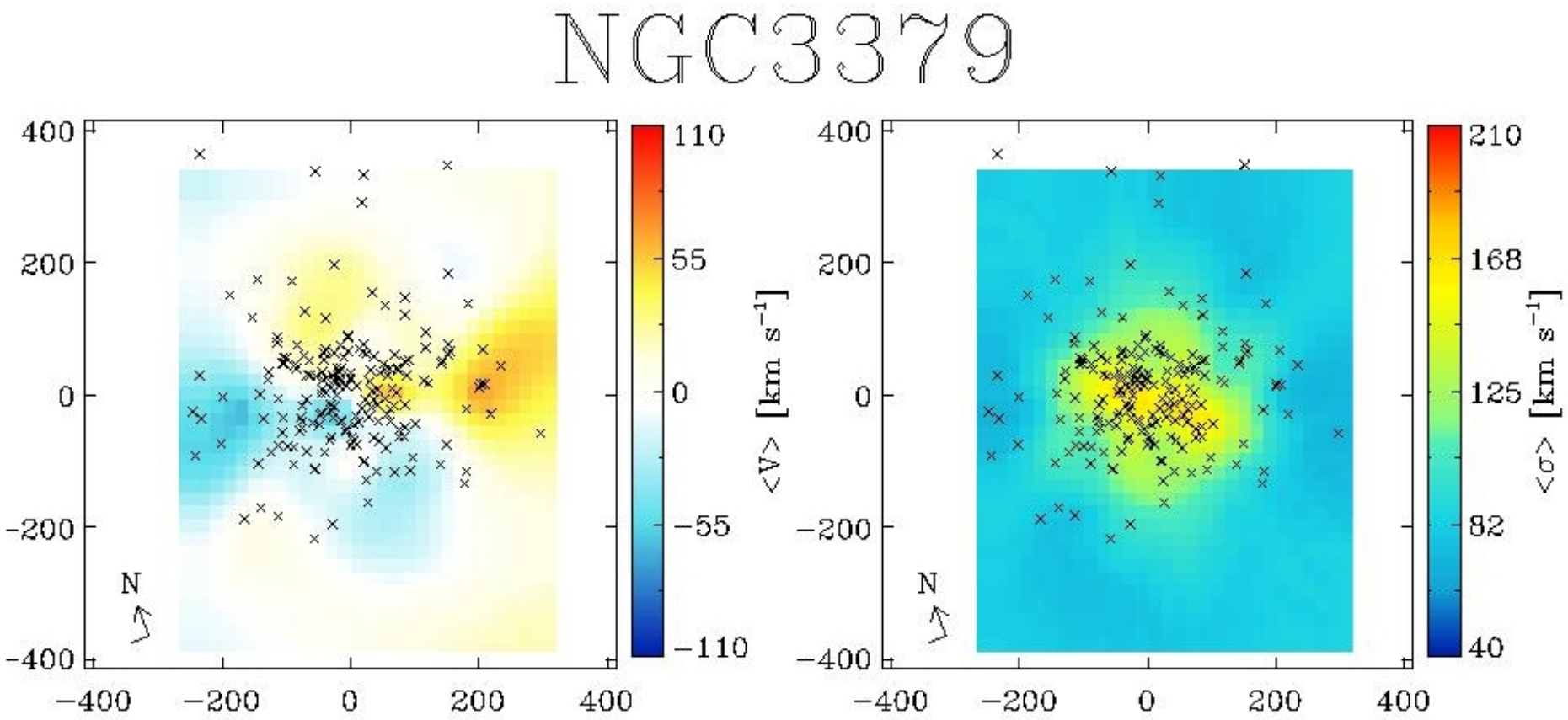
NGC3379
400
200
0
-200
-400
−400
−200
0
200
400
N
110
55
0
−55
−110
<V> [km s^{-1}]
210
168
125
82
40
<σ> [km s^{-1}]

Пример S0 с полярным балджем

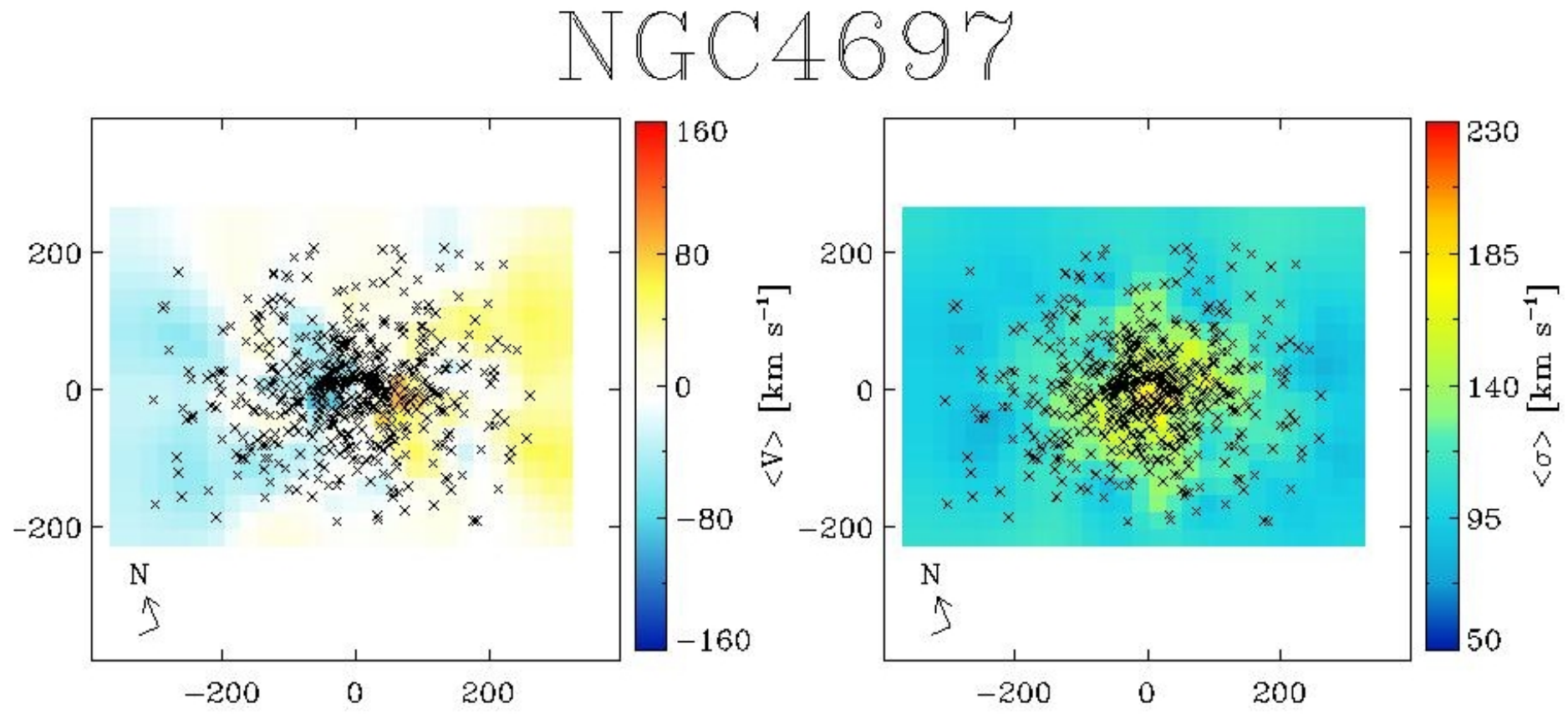

Astro-ph: 1712.06611

Major Merging History in CANDELS. I. Evolution of the Incidence of Massive Galaxy-Galaxy Pairs from $z = 3$ to $z \sim 0$

Kameswara Bharadwaj Mantha[1⋆], Daniel H. McIntosh[1], Ryan Brennan[2], Henry C. Ferguson[3], Dritan Kodra[4], Jeffrey A. Newman[4], Marc Rafelski[3], Rachel S. Somerville[2], Christopher J. Conselice[5], Joshua S. Cook[1], Nimish P. Hathi[3], David C. Koo[6], Jennifer M. Lotz[3], Brooke D. Simmons[7], Amber N. Straughn[8], Gregory F. Synder[3], Stijn Wuyts[9], Eric F. Bell[10], Avishai Dekel[11], Jeyhan Kartaltepe[12], Dale D. Kocevski[13], Anton M. Koekemoer[3], Seong-Kook Lee[14], Ray A. Lucas[3], Camilla Pacifici[15], Michael A. Peth[16], Guillermo Barro[17], Tomas Dahlen[3], Steven L. Finkelstein[18], Adriano Fontana[19], Audrey Galametz[20], Norman A. Grogin[3], Yicheng Guo[6], Bahram Mobasher[21], Hooshang Nayyeri[21], Pablo G. Pérez-González[22], Janine Pforr[23,24], Paola Santini[19], Mauro Stefanon[25], Tommy Wiklind[3].

Affiliations are listed at the end of this paper

Выборка

Table 1. Galaxy Sample Information. Columns: (1) name of the field/survey; (2) the total number of sources in photometry catalog before (after) applying good-source cuts described in Section 2.1.1; (3) the redshift range of interest in our study, used to select the mass-limited sample counts in (4,5), where the subsets with spectroscopic redshift information are given in parenthesis.

Name (1)	Phot Sources (2)	Redshift Range (3)	$\log_{10}(M_{\rm stellar}/M_\odot) \geq 9.7$ (4)	$\log_{10}(M_{\rm stellar}/M_\odot) \geq 10.3$ (5)
UDS	35932 (33998)	$0.5 \leq z \leq 3.0$	3019 (260)	1223 (141)
GOODS-S	34930 (34115)	$0.5 \leq z \leq 3.0$	2491 (892)	942 (403)
GOODS-N	35445 (34693)	$0.5 \leq z \leq 3.0$	2946 (494)	1133 (209)
COSMOS	38671 (36753)	$0.5 \leq z \leq 3.0$	3232 (11)	1307 (9)
EGS	41457 (37602)	$0.5 \leq z \leq 3.0$	2825 (199)	1093 (72)
CANDELS (Total)	186,435 (177,161)	$0.5 \leq z \leq 3.0$	14,513 (1856)	5698 (834)
SDSS-DR4 (1790 sq. deg)	141,564	$0.03 \leq z \leq 0.05$	9183 (8524)	4098 (3859)

Ограничения на выборки

2.3.1 Projected Separation

With our well-defined mass-limited samples for CANDELS and SDSS in hand, we start by identifying the massive ($M_{\rm stellar} \geq 2 \times 10^{10} M_{\odot}$) galaxies hosting a major projected companion satisfying $1 \leq M_1/M_2 \leq 4$ and a projected physical separation of 5 kpc $\leq R_{\rm proj} \leq$ 50 kpc. The choice of $R_{\rm proj} \leq 50$ kpc is common in close-pair studies (Patton & Atfield 2008; Lotz et al. 2011; de Ravel et al. 2011) which is supported by the numerical simulation results showing that major bound companions with this separation will merge within $\lesssim$1 Gyr. Additionally, source blending from smaller separations ($\lesssim$1.2 kpc) can cause incompleteness at $z \gtrsim 0.04$ for SDSS and at $z \gtrsim 2.5$ for CANDELS. Thus, we adopt a lower limit of $R_{\rm proj} = 5$ kpc ($\sim 4\times$ the resolution), which also corresponds to the typical sizes of $\log_{10}(M_{\rm stellar}/M_{\odot}) \geq 9.7$ galaxies at $2.0 \leq z \leq 2.5$. In summary, we find $N_{\rm proj} = 318$ and $N_{\rm proj} = 2451$ unique (i.e., duplicate resolved) massive galaxies hosting major projected companions in SDSS ($0.03 \leq z \leq 0.05$) and CANDELS (total of all five fields at $0.5 \leq z \leq 3.0$), respectively. We tabulate the breakdown of $N_{\rm proj}$ by redshift per each CANDELS field in Table 2.

Результат: после z=1 доля больших слияний падает

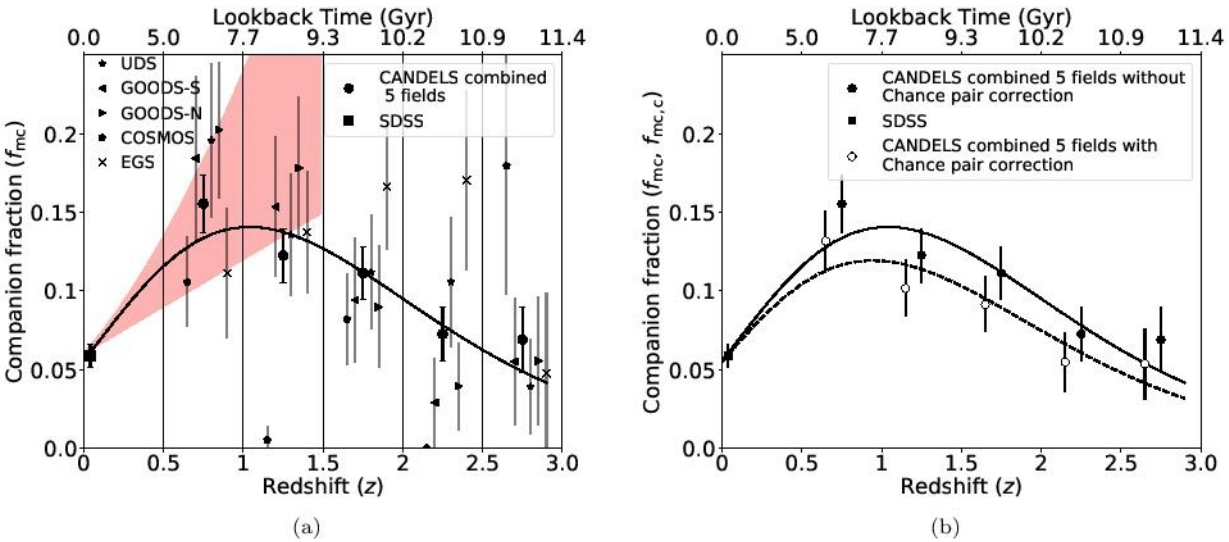

Figure 5. (a): The redshift evolution of the *major companion* fraction $f_{\rm mc}$ shown for the five CANDELS fields UDS (star), GOODS-S (left triangle), GOODS-N (right triangle), COSMOS (pentagon), EGS (cross). The combined CANDELS fractions in five redshift bins (circles) and the SDSS low-redshift anchor (square) include 95% binomial confidence limit error bars. To place our finding in the context of common, close-pair-based evolutionary trends found in the literature, we plot the shaded region (red) encompassing a common range of power-law slopes $f_{\rm mc} = 0.06(1+z)^{1-2}$ at $0 < z < 1.5$. (b): The random chance corrected fractions ($f_{\rm mc,c}$) for the five CANDELS Δz bins (open circles) are compared with the $f_{\rm mc}(z)$ from (a). For $f_{\rm mc,c}$, the binomial errors and scatter of C_3 (see § 3.3.3) are added in quadrature. Best-fit curves to the companion fraction ($f_{\rm mc}$) evolution data (see Equation 7 and § 3.3.2 for details) are shown in solid ($f_{\rm mc}$) and dashed ($f_{\rm mc,c}$) lines, respectively. In the case of SDSS, since the correction $C_3 \sim 0.01$, we only plot $f_{\rm mc}$ for simplicity. From this figure, we conclude that the major companion fraction increases strongly from $z \sim 0$ to $z \sim 1$, and decreases steeply towards $z \sim 3$ (see text for details).

Сравнение с предшественниками

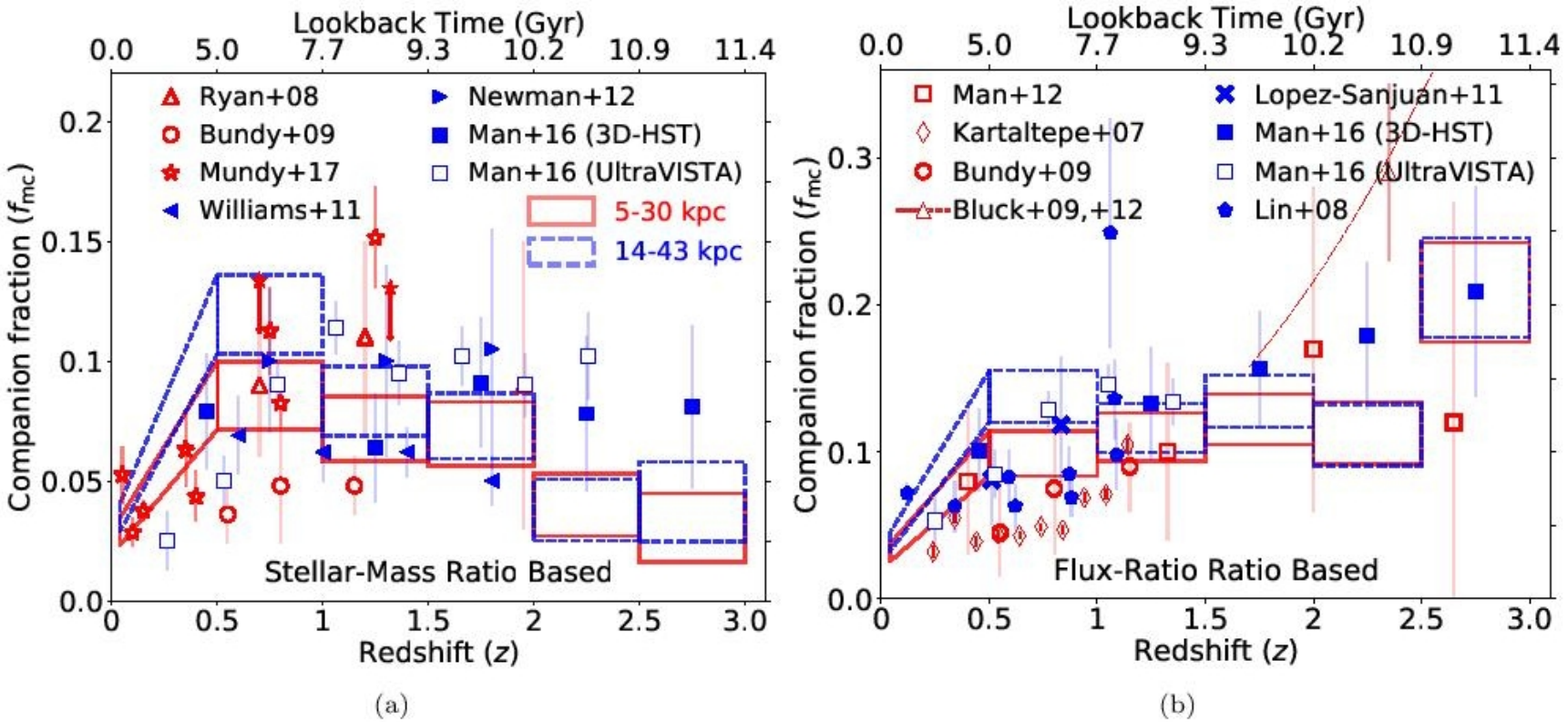

Figure 10. Comparison of major companion fractions from CANDELS+SDSS to those from previous studies that employed 4:1 stellar-mass ratio (a) and 4:1 flux-ratio (b) selections. In both panels, we outline the f_{mc} measurements data points as rectangles where their height represents the 95% binomial confidence limits per redshift bin (width of the rectangles). The data-points of previous empirical studies are given in the panel keys (see Table 5). We compare fractions based on different projected separation criteria as follows: $5-30$ kpc (solid-red line; open-red markers), and $14-43$ kpc (blue-dashed line, filled-blue markers). We find our major companion fraction estimates are in good agreement with previous empirical constraints when the companion selection criteria are closely matched. We off-set multiple fields from Mundy et al. (2017) by a small amount, and show the upper-limits in filled markers with bold arrow for clarity.

Противоречие теории

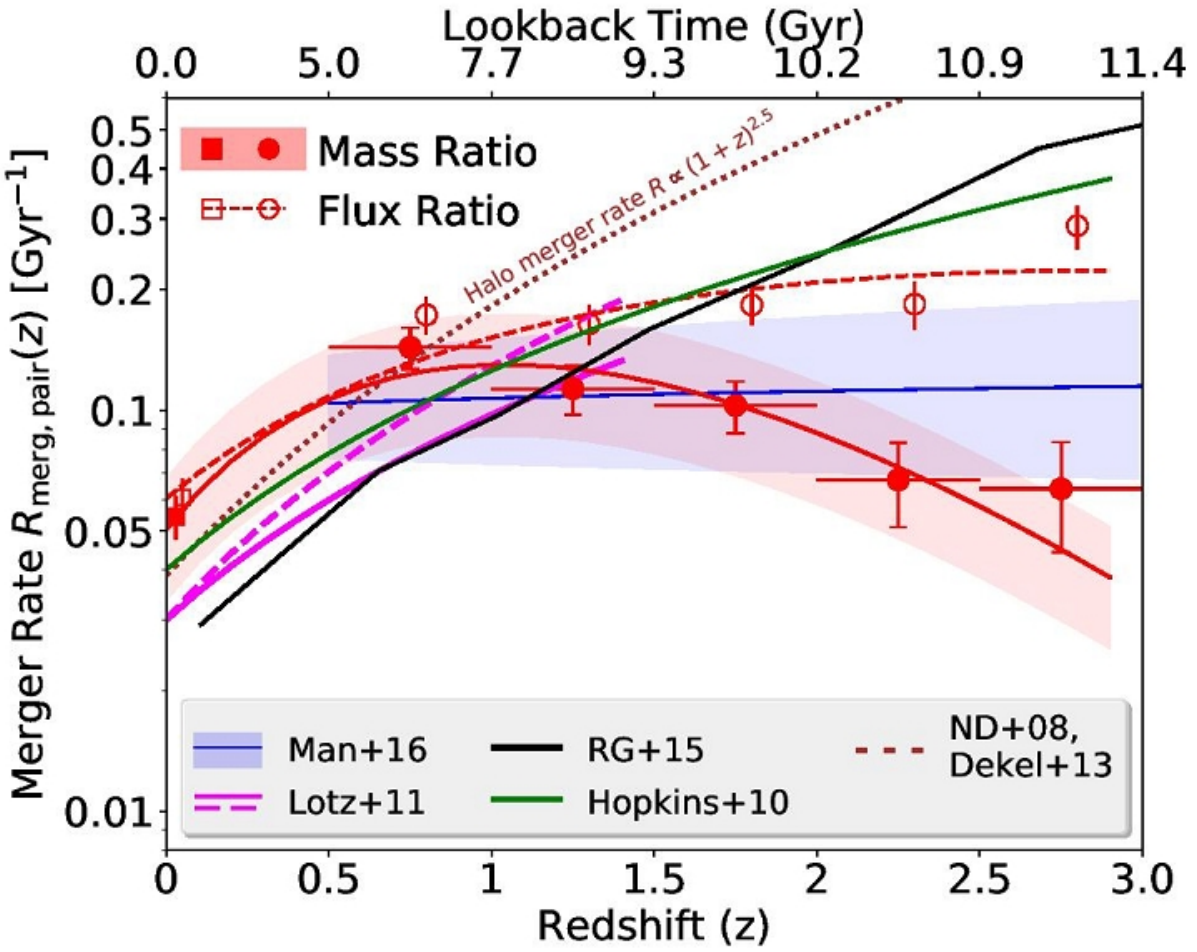

Figure 11. Comparison of CANDELS+SDSS galaxy-galaxy major merger rates $R_{\rm merg,pair}(z)$ (number of mergers per galaxy per Gyr) for massive ($M_{\rm stellar} \geq 2 \times 10^{10} M_{\odot}$) galaxies at $0 < z < 3$, to rates from previous empirical studies and theoretical model predictions. We show the $R_{\rm merg,pair}(z)$ computed using major companion fractions ($f_{\rm mc}$) based on fiducial projected separation ($5 - 50$ kpc) and redshift proximity (CANDELS: Equation 1; SDSS: $\Delta v_{12} \leq 500\,{\rm km\,s^{-1}}$) split into stellar mass-ratio (filled points; solid line) and flux ratio (open points; dashed line) for CANDELS (circles) and SDSS (square). We employ simplistic assumptions for fraction-to-rate conversion factors $T_{\rm obs,pair} = 0.65$ Gyr and $C_{\rm merg,pair} = 0.6$, and show the variation of $R_{\rm merg,pair}(z)$ for $C_{\rm merg,pair} = 0.4$ to 0.8 in red-shading. The error-bars on the data points indicate their 95% binomial confidence limits, solely based on the observed number counts. The solid

Как поправить положение: уменьшить время жизни пар на больших z

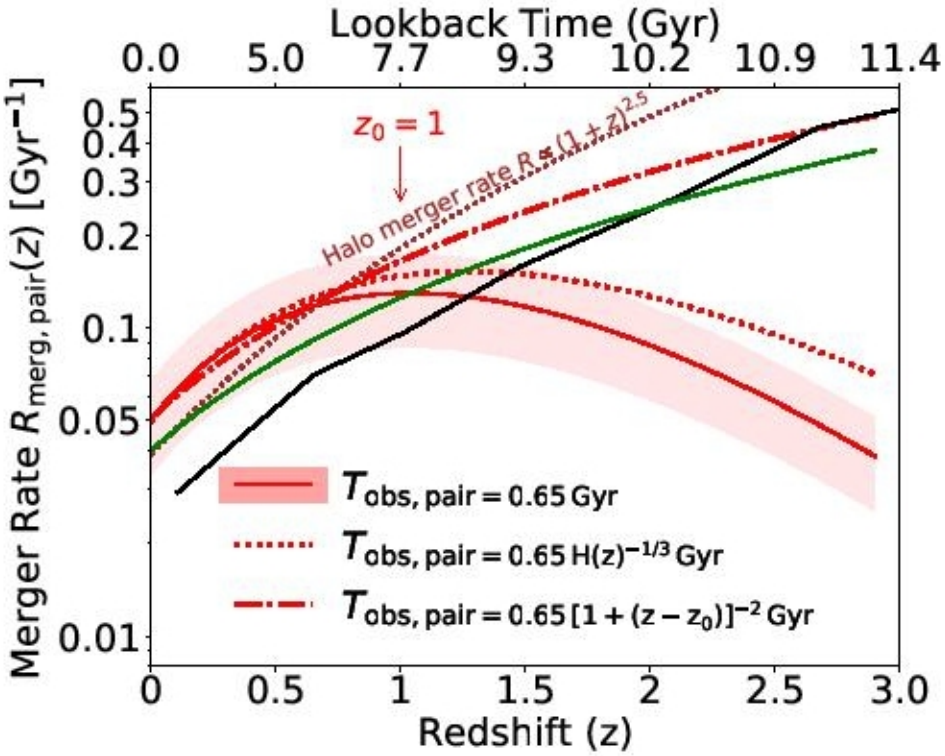

Figure 12. Comparing the redshift evolution of major merger rate of $M_{\rm stellar} \geq 2 \times 10^{10} M_{\odot}$ galaxies based on our fiducial close-pair timescale assumption $T_{\rm obs,pair} = 0.65$ Gyr copied from Figure 11 (solid red line, shading) to rates from different timescale choices. We show the rates based on Jiang et al. (2014) scaling relation $T_{\rm obs,pair} \propto H(z)^{-1/3}$ in red dotted line, and Snyder et al. (2017) relation $T_{\rm obs,pair} \propto (1+z)^{-2}$ in red dot-dashed line (starting at $z_0 = 1$). We also plot the theoretical merger rate predictions shown in Figure 11.

Astro-ph: 1712.06636

Deep neutral hydrogen observations of Leo T with the Westerbork Synthesis Radio Telescope

Elizabeth A. K. Adams[1,2] and Tom A. Oosterloo[1,2]

[1] ASTRON, Netherlands Institute for Radio Astronomy, Postbus 2, 7900 AA Dwingeloo, The Netherlands e-mail: adams@astron.nl
[2] Kapteyn Astronomical Institute, University of Groningen Postbus 800, 9700 AV Groningen, the Netherlands

December 20, 2017

ABSTRACT

Leo T is the lowest mass gas-rich galaxy currently known and studies of its gas content help us understand how such marginal galaxies survive and form stars. We present deep neutral hydrogen (H I) observations from the Westerbork Synthesis Radio Telescope in order to understand its H I distribution and potential for star formation. We find a larger H I line flux than the previously accepted value, resulting in a 50% larger H I mass of $4.1 \times 10^5\ M_\odot$. The additional H I flux is from low surface brightness emission that was previously missed; with careful masking this emission can be recovered even in shallower data. We perform a Gaussian spectral decomposition to find a cool neutral medium component (CNM) with a mass of $3.7 \times 10^4\ M_\odot$, or almost 10% of the total H I mass. Leo T has no H I emission extending from the main H I body, but there is evidence of interaction with the Milky Way circumgalactic medium in both a potential truncation of the H I body and the offset of the peak H I distribution from the optical center. The CNM component of Leo T is large when compared to other dwarf galaxies, even though Leo T is not currently forming stars and has a lower star formation efficiency than other gas-rich dwarf galaxies. However, the H I column density associated with the CNM component in Leo T is low. One possible explanation is the large CNM component is not related to star formation potential but rather a recent, transient phenomenon related to the interaction of Leo T with the Milky Way circumgalactic medium.

Карты в нейтральном водороде

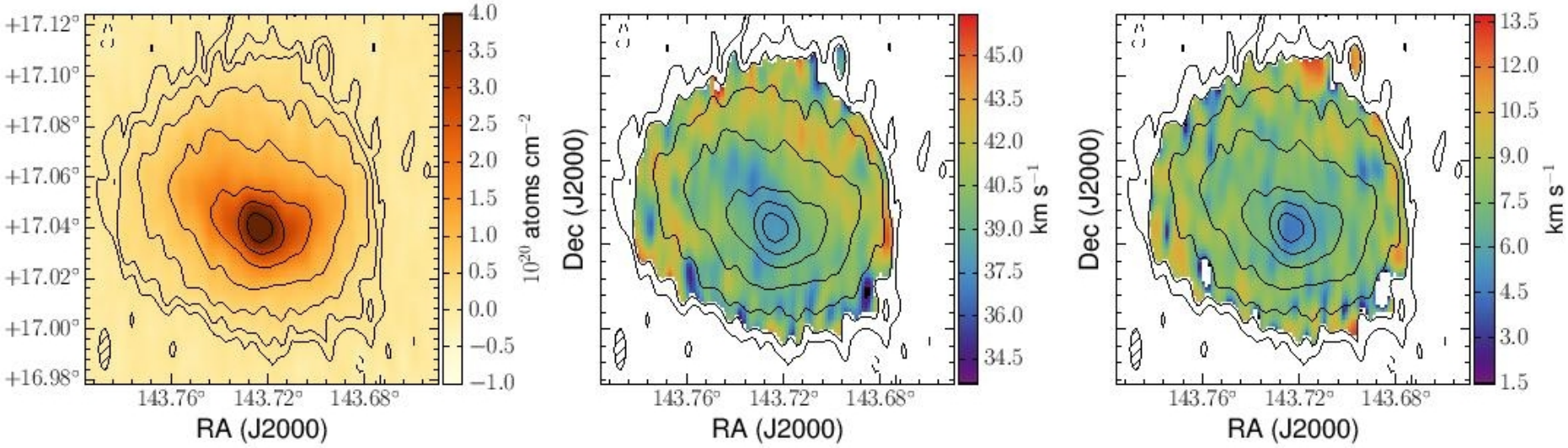

Fig. 2. Total intensity (primary-beam corrected), moment one (velocity field) and moment two (velocity dispersion) maps of Leo T. H I contours shown in each panel are [-1.5, 1.5, 2.5, 5, 10, 20, 30, 40] $\times 10^{19}$ atoms cm^{-2}; the lowest contour level is slightly below the 3-σ level.

Свойства галактики и результаты

Table 1. Properties of Leo T

Property	Value
Optical center	$9^h34^m53.4^s$ +17°03′05″
H I center	$9^h34^m54.0^s$ +17°02′52″
Distance	420 kpc
$S_{\rm int}$	9.9 ± 1.0 Jy km s^{-1}
$S_{\rm int,CNM}$	0.9 ± 0.2 Jy km s^{-1}
$S_{\rm int,WNM}$	9.0 ± 1.0 Jy km s^{-1}
$\sigma_{\rm CNM}$	2.5 ± 0.1 km s^{-1}
$\sigma_{\rm WNM}$	7.1 ± 0.4 km s^{-1}
$v_{\rm cen,CNM}$	37.4 ± 0.1 km s^{-1}
$v_{\rm cen,WNM}$	39.6 ± 0.1 km s^{-1}
$N_{\rm HI,peak}$	4.6×10^{20} atoms cm^{-2}
$a \times b^a$	3.3′× 3.0′
$r_{\rm HI}{}^a$	400 pc
$M_{\rm HI}$	$4.1 \pm 0.4 \times 10^5\ M_\odot$
$M_{\rm CNM}$	$0.37 \pm 0.08 \times 10^5\ M_\odot$
$M_{\rm WNM}$	$3.7 \pm 0.4 \times 10^5\ M_\odot$
$M_\star$	$2.0 \times 10^5\ M_\odot$
$M_{\rm dyn}{}^a$	$1.9 \times 10^7\ M_\odot$
$f_{\rm gas}$	0.73

Notes.^{a} H I extent is measured at the 2.7×10^{19} atoms cm^{-2} level.

Два компонента разной температуры?

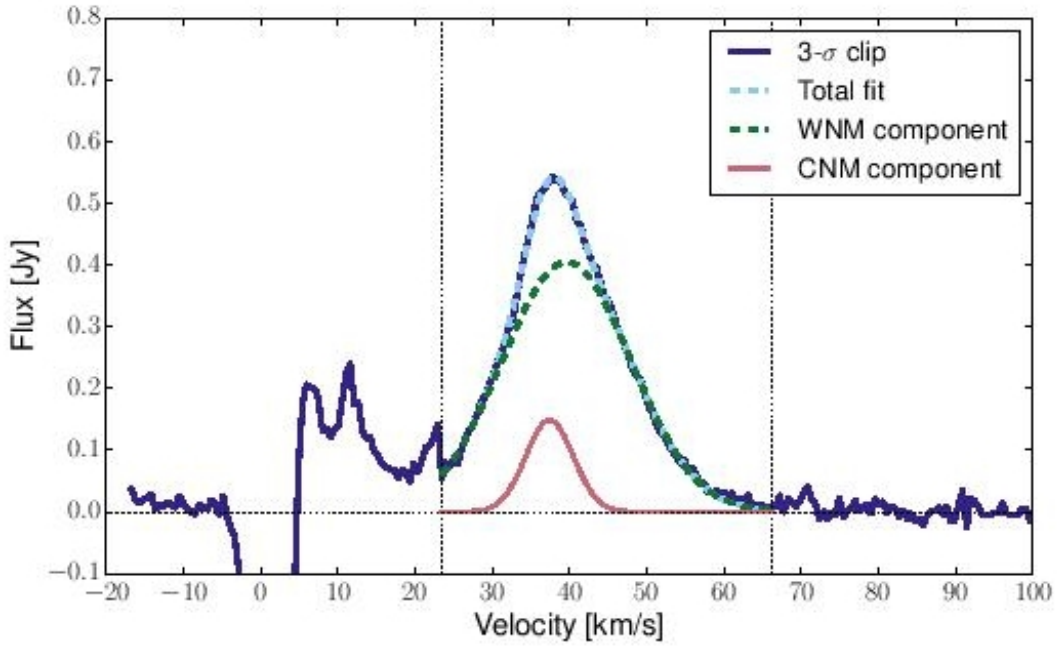

Fig. 3. Spectrum of Leo T based on a 3-sigma clip of the total intensity H I map. The velocity range used for constructing the total intensity H I map is shown by the dotted vertical lines. In addition, a two Gaussian component fit to this spectrum in shown.

Разное распределение и скорости компонент

CNM

WNM

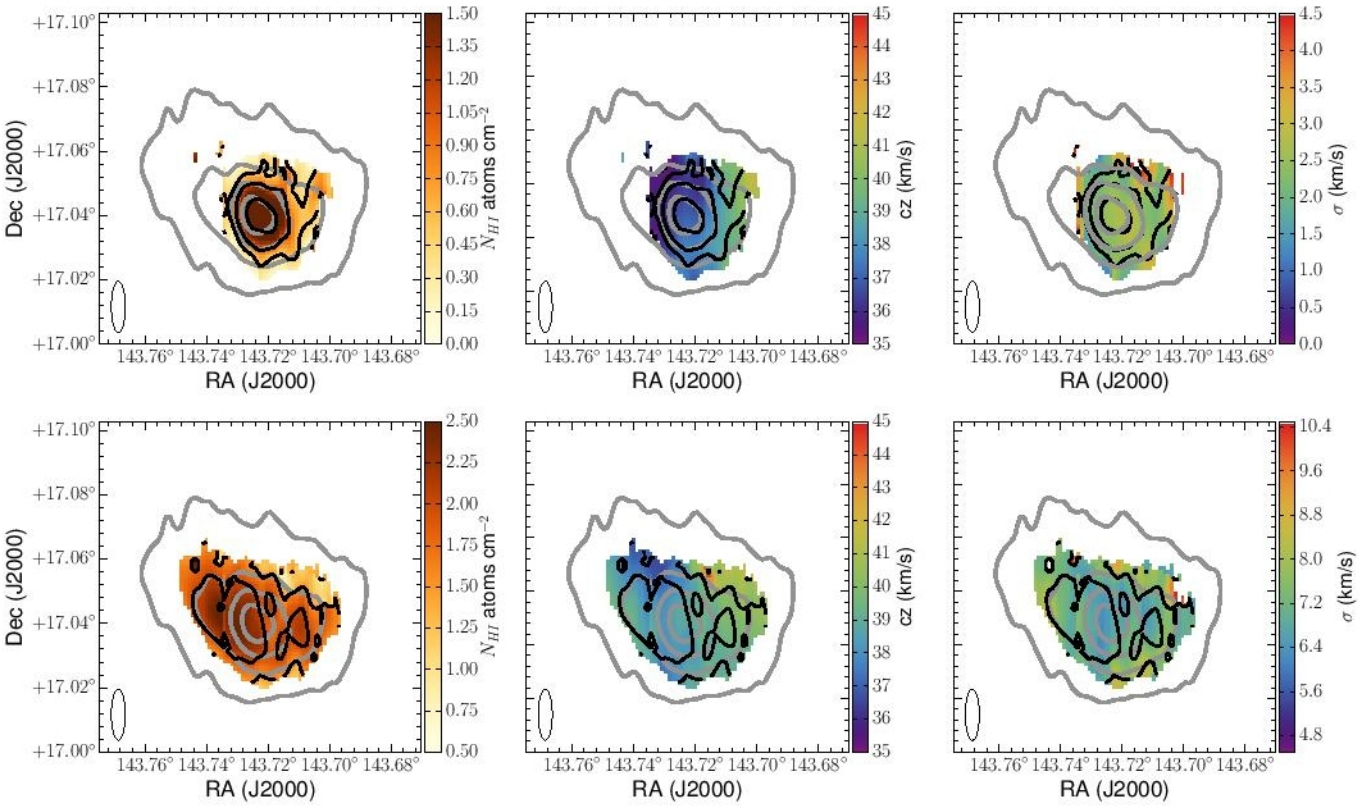

Асимметрия распределения газа

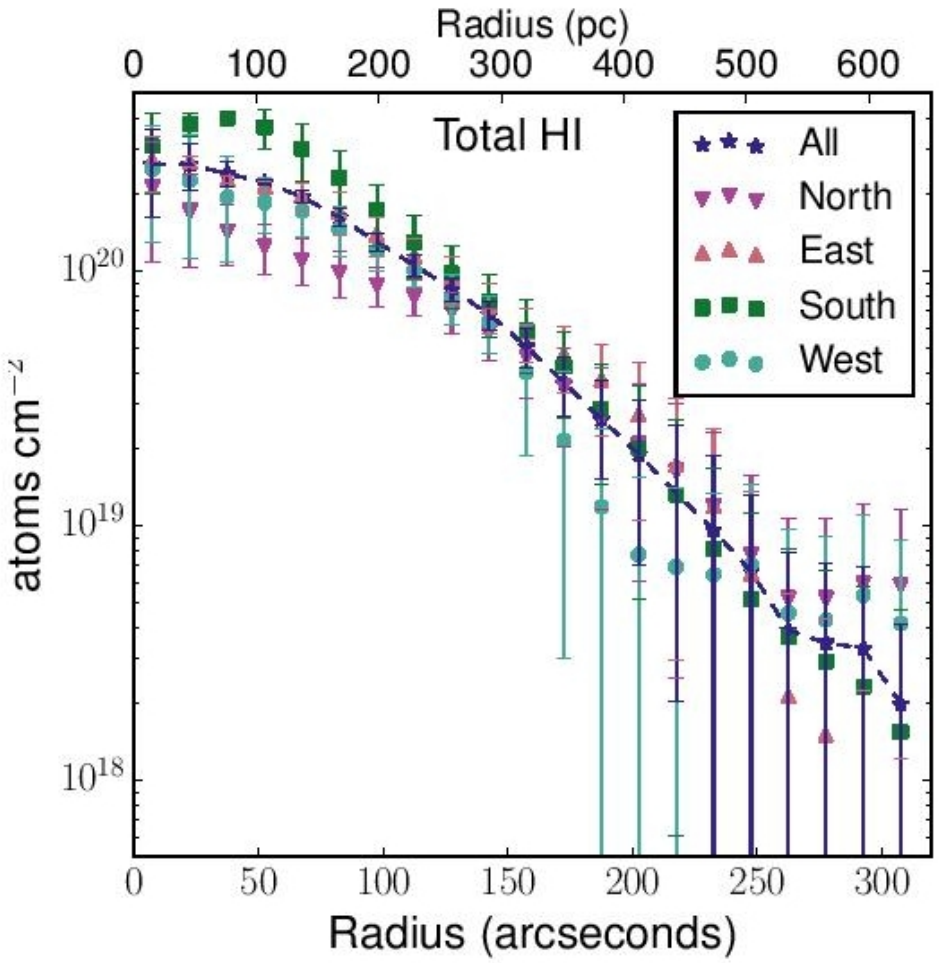

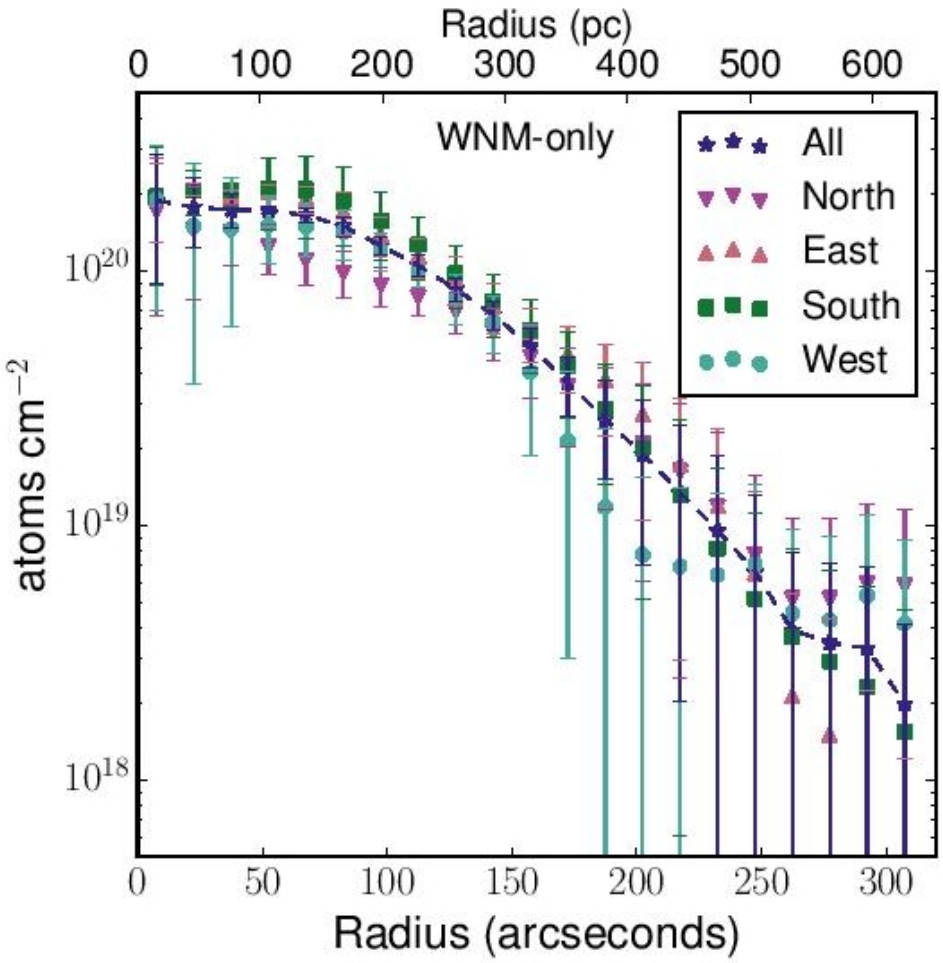

Astro-ph: 1712.07145

Revisiting Stephan's Quintet with deep optical images

Pierre-Alain Duc,[1]★ Jean-Charles Cuillandre [2] and Florent Renaud [3]
[1] *Université de Strasbourg, CNRS, Observatoire astronomique de Strasbourg, UMR 7550, F-67000 Strasbourg, France*
[2] *IRFU, CEA, Université Paris-Saclay, Université Paris Diderot, AIM, Sorbonne Paris Cité, CEA, CNRS, Observatoire de Paris, PSL Research University, F-91191 Gif-sur-Yvette Cedex, France*
[3] *Department of Astronomy and Theoretical Physics, Lund Observatory, Box 43, SE-221 00 Lund, Sweden*

Accepted for publication in MNRAS letters

ABSTRACT
Stephan's Quintet, a compact group of galaxies, is often used as a laboratory to study a number of phenomena, including physical processes in the interstellar medium, star formation, galaxy evolution, and the formation of fossil groups. As such, it has been subject to intensive multi-wavelength observation campaigns. Yet, models lack constrains to pin down the role of each galaxy in the assembly of the group. We revisit here this system with multi-band deep optical images obtained with MegaCam on the Canada-France-Hawaii Telescope (CFHT), focusing on the detection of low surface brightness (LSB) structures. They reveal a number of extended LSB features, some new, and some already visible in published images but not discussed before. An extended diffuse, reddish, lopsided, halo is detected towards the early-type galaxy NGC 7317, the role of which had so far been ignored in models. The presence of this halo made of old stars may indicate that the group formed earlier than previously thought.

Красное гало = старая срелаксированная группа

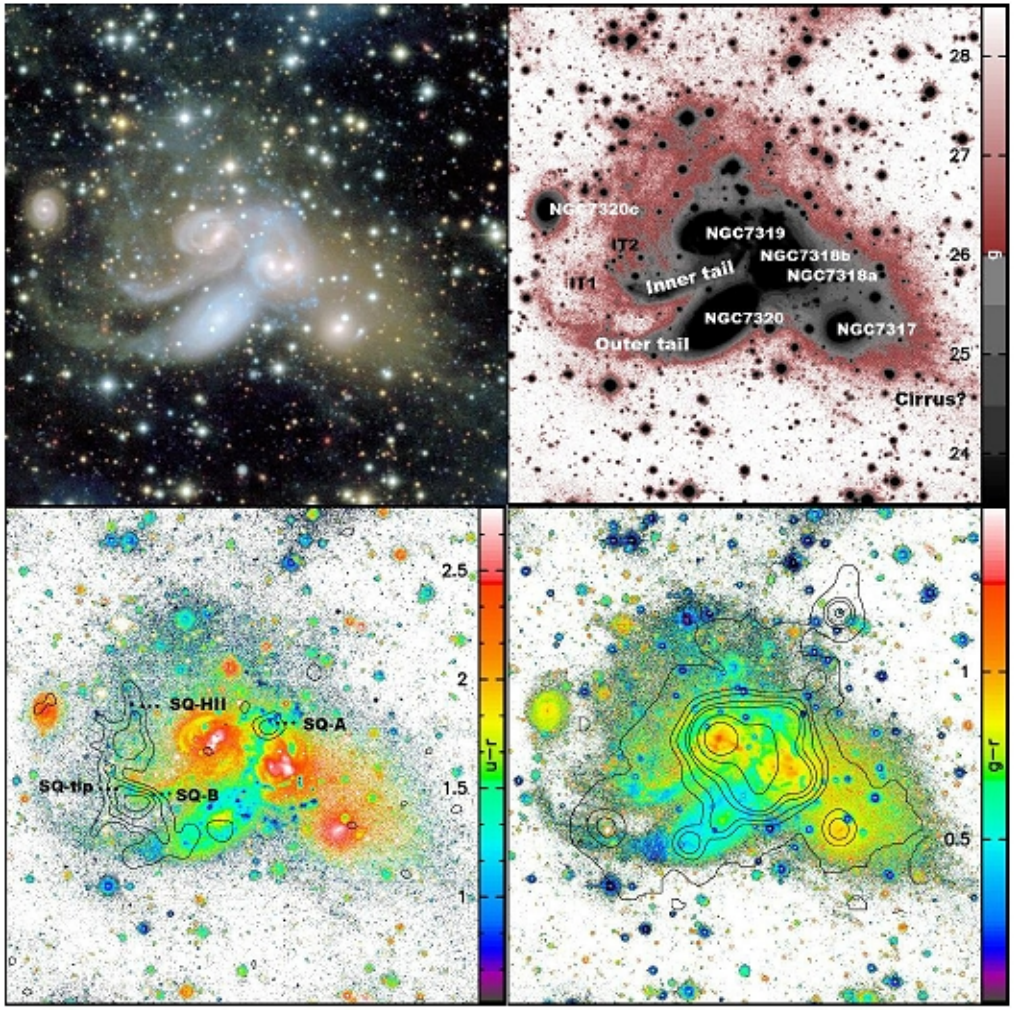

Figure 1. *Top-left*: composite u+g+r true colour image of the Stephan's Quintet. *Top-right*: g-band surface brightness map, with the principle structures labeled. The faintest emission (with surface brightness above 26 mag.arcsec^{-2}) revealed by the deep CFHT MegaCam image is shown in red. *Bottom-left*: u-r colour map with HI/VLA map in the velocity range 6475-6755 km.s^{-1} superimposed. The lowest contour is 6×10^{19} cm^{-2} (adapted from Williams et al. 2002). Selected intergalactic star-forming regions are labeled. *Bottom-right*: g-r colour map with archival X-ray/XMM-Newton contours superimposed. For the surface brightness and colour maps, the scale in mag resp. mag.arcsec^{-2} is indicated to the right. The field of view is 10' × 10' (250 kpc × 250 kpc). North is up and East left.